

Does electronic coherence enhance anticorrelated pigment vibrations under realistic conditions?

Hong-Guang Duan^{1,2,3}, Michael Thorwart^{2,3} & R. J. Dwayne Miller^{1,3,4}

¹*Max Planck Institute for the Structure and Dynamics of Matter, Luruper Chaussee 149, 22761, Hamburg, Germany*

²*I. Institut für Theoretische Physik, Universität Hamburg, Jungiusstraße 9, 20355 Hamburg, Germany*

³*The Hamburg Center for Ultrafast Imaging, Luruper Chaussee 149, 22761 Hamburg, Germany*

⁴*The Departments of Chemistry and Physics, University of Toronto, 80 St. George Street, Toronto Canada M5S 3H6*

April 9, 2019

The light-harvesting efficiency of a photoactive molecular complex is largely determined by the properties of its electronic quantum states. Those, in turn, are influenced by molecular vibrational states of the nuclear degrees of freedom. Here, we reexamine two recently formulated concepts that a coherent vibronic coupling between molecular states would either extend the electronic coherence lifetime or enhance the amplitude of the anticorrelated vibrational mode at longer times. For this, we study a vibronically coupled dimer and calculate the nonlinear two-dimensional (2D) electronic spectra which directly reveal electronic coherence. The timescale of electronic coherence is initially extracted by measuring the anti-diagonal bandwidth of the central peak in the 2D spectrum at zero waiting time. Based on

the residual analysis, we identify small-amplitude long-lived oscillations in the cross-peaks, which, however, are solely due to groundstate vibrational coherence, regardless of having resonant or off-resonant conditions. Our studies neither show an enhancement of the electronic quantum coherence nor an enhancement of the anticorrelated vibrational mode by the vibronic coupling under ambient conditions.

In the initial steps of photosynthesis, photoactive molecular complexes capture the sunlight energy and transfer it to the reaction center on an ultrafast time scale and with unity quantum efficiency ¹. The performance is determined by the molecular electronic properties, in concert with the molecular vibrations and coupling to the environment given by a solvent and the surrounding pigments and proteins. To investigate the energy transfer, ultrafast 2D electronic spectroscopy ²⁻⁴ is able to resolve fs time scales. It is able to reveal the interactions between the energetically close-lying molecular electronic states, for which the linear spectra are commonly highly congested and broadened by the strong static disorder ⁵. Recent experimental studies of the Fenna-Matthews-Olson (FMO) complex reported long-lived oscillations of the cross-peaks both at low ⁶ and at room temperature ⁷ which have been assigned to enhanced electronic coherence. This has generated tremendous interest in this new field of quantum biology ⁸, aiming to reveal a functional connection between photosynthetic energy transfer and long-lived quantum coherence. Moreover, also in photoactive marine cryptophyte algae ⁹, the light-harvesting complex LHCII ¹⁰ and in the Photosystem II reaction center ^{11,12}, long-lived oscillations have been experimentally reported at low and room temperature.

To model the reported ⁶ coherence, Ishizaki and Fleming have used a parametrized model of the FMO complex ¹³, with a rather small reorganization energy of 35 cm^{-1} to fit the electronic coherence timescale ¹⁴. This value was extracted ¹⁵ from fluorescence line narrowing measurements at low temperature ¹⁶ and does not include high-frequency intramolecular modes. However, even with the small reorganization energy, Shi *et al.* have calculated the complete 2D spectra and found a much shorter electronic coherence lifetime ¹⁷. They have pointed out that the interpretation of the long-lived coherence could just be due to the intentional magnification of the 2D spectral amplitudes by the deliberately used inverse hyperbolic sine scale. In addition, electronic quantum coherence has been questioned to play any crucial role for the energy transfer as the transport is dominated by largely incoherent exciton relaxation ^{18,19}. A critical issue has been the use of an inadequate spectral distribution of the environmental fluctuations. The experimentally determined spectral density with a larger reorganization energy ¹⁵ has been used to calculate the dynamics by the quadiabatic propagator path integral ¹⁸. There, a local vibrational mode at 180 cm^{-1} with a broadening of 29 cm^{-1} has been included, with a total reorganization energy of 100 cm^{-1} . The numerically exact results also show a significantly shorter electronic coherence lifetime. Recent QM/MM-simulations ²⁰⁻²⁴ yield site-resolved spectral densities with reorganization energies of 150 to 200 cm^{-1} .

Thus, theoretical studies showed that pure electronic quantum coherence can not survive under ambient conditions. Motivated by this disagreement, the coherent exciton dynamics in the FMO complex has been reexamined experimentally by 2D electronic spectroscopy ²⁵. A fit to an Ohmic spectral density with a broadened high-frequency mode yields a reorganization energy of

190 cm⁻¹. The observed lifetime of the electronic coherence of ~60 fs is too short to play any functional role in the energy transport, which occurs of the ps time scale.

In addition to the electronic coherence, signatures of the vibrational coherence of the pigment-protein host can also be accessed on the same spectroscopic footing²⁶⁻²⁹. Yet, electronic coherence can be distinguished from vibrational coherence^{30,33,34}. Long-lived pure electronic coherence is unexpected to exist in most light harvesting complexes. However, long-lived vibrational coherence is common and is not expected to strongly affect light harvesting in the first place. Two concepts are currently under debate: i) In 2013, Plenio *et al.*³¹ argued that long-lived vibrationally coherent modes can significantly enhance the electronic coherence lifetime when the vibrational and electronic degrees of freedom are resonantly coupled. The vibrational mode thereby is supposed to act as a “phonon laser” on the excitons, thereby producing ultralong electronic coherence. ii) Moreover, Tiwari *et al.*³² argued that nonadiabatic electronic-vibrational coherent mixing at short times resonantly enhance the amplitude of the particular delocalized anticorrelated vibrational mode on the ground electronic state. This second concept does not involve long-lived electronic coherence and is conceptually in agreement with the observation that a strong vibronic coupling produces large-amplitude coherent oscillations of the electronic component with a usual short lifetime and a long-lived vibrational coherence, but with a rather small amplitude^{33,34}. This scenario was re-examined again recently³⁵ with an explicit coupling to an electronic and a vibrational bath. The result that an increased vibronic coupling survives weak electronic dephasing at short times and induces a resonantly enhanced long-lived vibrational coherence of the anticorrelated mode was presented as an explanation of the long-lived coherence signals observed in Ref. ⁶. However,

again, an unrealistically weak electronic damping with a reorganization energy of 35 cm^{-1} has been used.

Motivated by this discrepancy, we have reexamined the coherent dynamics in a model of a vibronically coupled excitonic dimer with anticorrelated pigment vibrations. We calculate the 2D electronic spectra of the model dimer as being part of the FMO complex. We use the environmental parameters obtained from the recent FMO experiment²⁵. We examine the electronic coherence lifetime by the antidiagonal bandwidth of the diagonal peak at zero waiting time. The oscillations in the residuals obtained from the global fitting analysis confirm that the long-lived coherence is purely vibrational in nature, irrespective of resonant or non-resonant conditions. To distinguish the coherent dynamics of the electronic excited state, we have calculated the dynamics of the electronic wave-packet on the vibrational potential energy surfaces (PESs), accompanied by the projection onto the reaction coordinates. Also here, the vibrational coherence is clearly identified by the oscillations close to the potential minimum. The projection shows that the long-lived oscillations are solely of vibrational origin, which confirms the 2D spectroscopic calculations. Moreover, we show that under realistically strong electronic damping, coherent vibronic coupling at short times does not enhance the amplitude of the anticorrelated vibrational mode, while we recover the mechanism of vibronic enhancement only for unrealistically weak electronic damping.

Theory

The model is described by a total Hamiltonian consisting of the system, bath and the system-bath interaction terms, $H = H_S + H_{SB}$. The system is a dimer consisting of monomer A and B with site energies $E_{A/B}$, both having the same electronic ground state $|g\rangle$ and the respective electronic single excited states $|A\rangle$ and $|B\rangle$. The double excited state is denoted as $|AB\rangle$. Each electronic excited state couples to a vibrational mode (each to its own mode). The two couplings are such that an anticorrelated out-of-phase oscillation of the two electronic states occurs. In the exciton site basis, we have

$$\begin{aligned}
 H_S = & |g\rangle h_g \langle g| + |A\rangle h_A \langle A| + |B\rangle h_B \langle B| \\
 & + (|A\rangle V \langle B| + h.c.) + |AB\rangle (h_A + h_B) \langle AB| .
 \end{aligned} \tag{1}$$

Here, $h_g = \frac{1}{2}\Omega(P_{A/B}^2 + Q_{A/B}^2)$, $h_A = E_A + h_g - \kappa Q_A$ and $h_B = E_B + h_g + \kappa Q_B$, respectively. $P_{A/B}$ and $Q_{A/B}$ are the momenta and the coordinates of the two vibrational modes coupled to monomer A and B. We express the vibronic coupling strength between ground and excited state as $\kappa = \frac{\Omega\Delta}{\sqrt{2}}$, where Δ is the dimensionless shift of the excited state relative to its ground state. Ω is the vibrational frequency (both modes are taken with equal characteristics). V denotes the electronic coupling between two electronic excited states $|A\rangle$ and $|B\rangle$.

For the discussion of the anticorrelated vibrations, it is useful to define new coordinates and momenta according to $Q_{\pm} = \frac{1}{\sqrt{2}}(Q_A \pm Q_B)$, and $P_{\pm} = \frac{1}{\sqrt{2}}(P_A \pm P_B)$ ³⁶. Then, the system

Hamiltonian can be written as

$$\begin{aligned}
H_S &= \sum_{n=0,1,2} H_{S,n} = \sum_{n=0,1,2} (H_{S,n}^+ + H_{S,n}^-), \\
H_{S,0}^- &= \mathbf{1}_0 h^-, \\
H_{S,1}^- &= \mathbf{1}_1 h^- + (E_B - \Omega Q_- \Delta / \sqrt{2}) |B\rangle \langle B| \\
&\quad + (E_A + \Omega Q_- \Delta / \sqrt{2}) |A\rangle \langle A| \\
&\quad + V(|A\rangle \langle B| + |B\rangle \langle A|), \\
H_{S,2}^- &= \mathbf{1}_2 (h^- + E_A + E_B), \tag{2}
\end{aligned}$$

with $[H_{S,n}^+, H_{S,n}^-] = 0$ and $H_{S,n}^+ = \mathbf{1}_n (h^+ - n\Omega Q_+ \Delta / \sqrt{2})$. The two rotated vibrational modes are given by $h^\pm = \frac{1}{2}\Omega(P_\pm^2 + Q_\pm^2)$ and the projection operators are $\mathbf{1} = \sum_{n=0,1,2} \mathbf{1}_n$, with $\mathbf{1}_0 = |g\rangle \langle g|$, $\mathbf{1}_1 = |A\rangle \langle A| + |B\rangle \langle B|$, and $\mathbf{1}_2 = |AB\rangle \langle AB|$.

We choose the same parameters as in Ref. ³² for the system Hamiltonian. This dimer mimics one exciton pair of the FMO complex. The bath part will be discussed below (in particular, we do not choose the same parameters of too weak damping, but use our own parameters of Ref. ²⁵). The electronic energy gap is set to $E_A - E_B = 150 \text{ cm}^{-1}$ and the electronic coupling is $V = 66 \text{ cm}^{-1}$. Moreover, the dimensionless vibrational shift is set to $\Delta = 0.2236$. The pure electronic energy gap without coupling can then be calculated to be $\Delta E = 200 \text{ cm}^{-1}$. As in Ref. ³², we model inhomogeneous broadening by a static Gaussian disorder of width $\delta E = 26 \text{ cm}^{-1}$. For the vibrational mode, we choose the frequency $\Omega = 200 \text{ cm}^{-1}$ which corresponds to the resonant case when the vibronic coupling vanishes (the slight shift of this resonance due to the vibronic coupling does not alter the overall result since we find essentially the same conclusion also for the

off-resonant case, see below).

The environment and coupling part $H_{SB} = H_{SB}^{\text{vib}} + H_{SB}^{\text{el}}$ consist of two parts, the vibrational baths which damp the vibrational motions, and the electronic bath which generates electronic dephasing and damping. In general, we assume Gaussian fluctuations described in terms of the standard model of dissipative quantum systems. The electronic environment is generated by fluctuating charges in the protein and the solvent and consists of two harmonic oscillator baths each of which couples to the electronic excited states of monomer A and B, respectively. Thus, we have the Hamiltonian $H_{SB}^{\text{el}} = \sum_{\alpha=A,B} H_{SB,\alpha}^{\text{el}}$ with

$$H_{SB,\alpha}^{\text{el}} = \frac{1}{2} \sum_{i=1}^N \left[\frac{p_{i,\alpha}^2}{m_{i,\alpha}} + m_{i,\alpha} \omega_{i,\alpha}^2 \left(x_{i,\alpha} - \frac{c_{i,\alpha} |\alpha\rangle \langle \alpha|}{m_{i,\alpha} \omega_{i,\alpha}^2} \right)^2 \right]. \quad (3)$$

As usual, $p_{i,\alpha}$ and $x_{i,\alpha}$ are the momenta and the coordinates of the i th bath mode coupling to the electronic state $\alpha = A, B$. For the electronic part, we choose an Ohmic spectral density with the parameters obtained from fitting the linear spectra of the FMO complex to experimental data, see Ref. ²⁵. Notice that these values correspond to much stronger damping than those in Ref. ³². Thus, each bath is assumed to have its own, but equal spectral density $J^{\text{el}}(\omega) = \gamma^{\text{el}} \omega \exp(-\omega/\omega_c)$, with $\gamma^{\text{el}} = 0.7$, $\omega_c = 350 \text{ cm}^{-1}$.

The vibrational environment roots in fluctuating nuclear degrees of freedom of the protein and couples to the vibrational displacements Q_A or Q_B of the mode coupled to the electronic state A or B. Hence, $H_{SB}^{\text{vib}} = \sum_{\alpha=A,B} H_{SB,\alpha}^{\text{vib}}$ with

$$H_{SB,\alpha}^{\text{vib}} = \frac{1}{2} \sum_{i=1}^N \left[\frac{q_{i,\alpha}^2}{\mu_{i,\alpha}} + \mu_{i,\alpha} \nu_{i,\alpha}^2 \left(y_{i,\alpha} - \frac{d_{i,\alpha} Q_\alpha}{\mu_{i,\alpha} \nu_{i,\alpha}^2} \right)^2 \right]. \quad (4)$$

$q_{i,\alpha}$ and $y_{i,\alpha}$ are the momenta and the coordinate of the i th vibrational bath mode of the state $\alpha = A, B$. We assume that the vibrational bath has the same spectral density as the electronic bath, i.e., $J^{\text{vib}}(\omega) = \gamma^{\text{vib}}\omega \exp(-\omega/\omega_c)$ but with weaker damping, $\gamma^{\text{vib}} = 0.02$ and $\omega_c = 350 \text{ cm}^{-1}$.

To disentangle electronic and vibrational coherence, we perform a projection of the electronic wave packet on the reaction coordinate, which allows us to distinguish the vibrational coherence from the vibronic dynamics. We assume the initial wave packet to be in the lowest vibrational state $|0\rangle$ of the electronic excited state $|A\rangle$ in the site basis, such that the initial density matrix can be written as $\rho(0) = |A, 0\rangle \langle A, 0|$. In order to obtain dynamical information, we determine the probability of the wave packet along the reaction coordinate Q_- by the time-dependent projection

$$P_k^{ad}(Q_-, t) = \langle Q_- | \langle \tilde{k} | \rho(t) | \tilde{k} \rangle | Q_- \rangle , \quad (5)$$

where P_k^{ad} is the probability density of the reaction coordinate and \tilde{k} indicates the electronic state of A or B in the exciton basis (for details of the projection, see Refs. ^{37,38}).

Results and Discussion

We assume ³² that two perpendicular transitions from the common ground state to the two excited states of monomer A and B are possible. Hence, the transition dipole moments are fixed to $\vec{\mu}_A = \mu_A \mathbf{e}_x$ and $\vec{\mu}_B = \mu_B \mathbf{e}_y$ with $\mu_A = \mu_B = 1$. Here, \mathbf{e}_j is the unit vectors in the direction j . Temperature is set to 300 K, if not stated otherwise. We use the time non-local quantum master equation ³⁹⁻⁴¹ with the equation-of-motion phase-matching-approach ⁴². Details are given in the

Supplementary Information Appendix of Ref. ²⁵.

We first consider the vibronic dimer with resonant vibrational coupling for which we obtain the 2D electronic spectrum shown in Fig. 1(A) (real part). At waiting time $T = 0$ fs, the inhomogeneous broadening can be clearly identified because the spectrum is stretched along the diagonal. It disappears within 50 fs (see the time dependent 2D electronic spectra in the SI). The corresponding 2D spectrum of the purely electronic dimer without vibrational modes is shown in Fig. 1(B). From the profiles taken along the antidiagonal band and shown in Figs. 1 (C) and (D), we observe that the anti-diagonal broadening of the 2D spectra in both cases is similar, which proves that both dimers undergo a similar dephasing dynamics with similar time scales of the electronic dephasing. They are extracted to be 70 fs and 80 fs, respectively. To resolve the time-dependent energy transfer, we analyze the series of 2D spectra for increasing waiting times, by the global fitting approach, see Supplementary Information Appendix for details. This yields the shortest lifetime of the decay associated spectra which is induced by the peak broadening and by electronic dephasing. Both lifetimes coincide in both cases which shows that a vibronic coupling does not alter the short-time electronic dephasing properties.

For a quantitative analysis of the dissipative dynamics in the presence of a vibrational coupling, we plot in Fig. 1 (E) the time evolution of the magnitude of the peaks selected in Fig. 1 (A). We observe that the dynamics can be clearly separated into two sectors: (i) fast electronic dephasing, which initially occurs on the time scale of ~ 70 fs, as already resolved by the analysis of the anti-diagonal bandwidth and the global fitting approach. Moreover, (ii) long-lived oscillations with

small amplitudes are resolved at longer times. In order to identify the origin of these long-lived oscillations, we perform a Fourier transform of the residual, which is obtained by subtracting the kinetics resolved by the global fitting. The result is shown in Figs. 1 (F) and (G). The process of fast electronic dephasing is associated to the broad background spectral band with a maximum at 200 cm^{-1} . In addition, this broad band is overlapped by one sharp peak at the same frequency of 200 cm^{-1} . One additional narrow peak is resolved at 400 cm^{-1} . It originates from the vibrational coherence between the vibrational ground $|0\rangle$ and the second vibrational level $|2\rangle$ of the electronic ground state, i.e., is of pure vibrational origin. This is further illustrated in Fig. S3 of the Supplementary Information Appendix, where the stick spectrum also indicates the clearly separated electronic and vibrational parts of which the eigenstates are composed. Hence, as a matter of fact, we can conclude that these narrow peaks at 200 cm^{-1} and 400 cm^{-1} only stem from vibrational coherence of each monomer.

Off-resonance case Up to here, we have studied the vibronic dimer for the resonant case $\Delta E = \Omega$. Next, we investigate the off-resonant case as well and choose $\Omega = 500\text{ cm}^{-1}$. The results are shown in Fig. 2 (A), the global fitting analysis is shown in the Supplementary Information Appendix. The fast electronic dephasing with the time scale of 69 fs is still present. It agrees with the value of the antidiagonal bandwidth (see the SI). Importantly enough, it coincides with the dephasing time scale of the resonant case. Hence, the fact that the electronic and vibrational dynamics are off-resonant does not affect the conclusion reached for the resonant case. In addition, we show in Fig. 2 (B) the dynamics of the selected peaks for growing waiting times. It shows the same kinetics as in the resonant case: One fast electronic dephasing component is combined with a

long-lived vibrational coherent component with a small amplitude. Again, we perform the Fourier transform of the residuals and plot the spectra of each peak in Fig. 2 (C). We again find one broad band with a maximum at 200 cm^{-1} , which manifests the fast electronic dephasing and coincides with the lifetime of $\sim 70 \text{ fs}$ resolved by the global fitting approach. One clearly separated narrow peak is located at 500 cm^{-1} with a large magnitude which is associated to the long-lived vibrational coherence. A clear evidence for the purely vibrational (and not vibronic) origin of the peak is that one additional peak can be resolved at $\sim 1000 \text{ cm}^{-1}$. It is the clear signature of the vibrational coherence between the vibrational ground $|0\rangle$ and the second vibrationally-excited level $|2\rangle$ on the electronic ground-state surface.

Low-temperature case Next, we consider the case of low temperature of 80 K. We follow the same steps as above and find for vanishing vibronic coupling $\kappa = 0$ an electronic dephasing time scale of 161 fs, see Fig. S4 in the SI. In the presence of a resonant vibrational mode with $\Omega = 200 \text{ cm}^{-1}$ and with $\kappa \neq 0$ set to the same value as above, we obtain the dephasing time of 121 fs, see Fig. S3 (B) in the SI. It is slightly smaller than the one of the purely electronic case, but still comparable. The dynamics of the selected peaks in the 2D spectra again shows long-lived oscillations, see Fig. S3 (C) of the SI. The Fourier transform, shown in Fig. S3 (D), shows again one sharp peak at 200 cm^{-1} , and one additional peak at 400 cm^{-1} with a quite weak magnitude. They manifest again the vibrational origin of the coherence. Therefore, we can conclude that, also for low temperature, the long-lived oscillation is just of vibrational origin. No different mechanism between low and room temperature occurs.

Vibrational dynamics of the monomer In addition to the dimer, we also investigate the monomer where only vibrational coherence is present. In Fig. S5 (B), we show the time trace of the selected cross peak together with the Fourier spectrum in (C). The spectra are dominated by one peak at the vibrational frequency. An additional peak appears at the position of twice the vibrational frequency. Thus, the same scenario occurs for the monomer as well. We clearly demonstrate that the long-lived oscillations in a vibronically-coupled dimer are just due to the overlap of the short-lived electronic coherence and the long-lived vibrational coherence.

Wave packet tracking A further confirmation of this picture is obtained from monitoring the dynamics of the electronic excited states. For this, we project the time-evolved density matrix onto the anticorrelated vibrational coordinate Q_- . We use the same parameters as before and calculate the PESs of the electronic excited states $|\tilde{A}\rangle$ and $|\tilde{B}\rangle$ in the adiabatic basis. The result for the off-resonant case with $\Omega = 500 \text{ cm}^{-1}$ is shown in Figs. 3 (A) to (D). The initial wave packet is prepared in the excited state $|A\rangle$. For growing time, the transfer of population from $|\tilde{A}\rangle$ to $|\tilde{B}\rangle$ can be clearly identified by the decrease of the magnitude in Fig. 3 (A) and the corresponding growth in Fig. 3 (B). By this, the vibrational coherence of the excited states is clearly visible from the oscillations around the potential minimum, see Fig. 3 (A). The oscillations have a period of ~ 66 fs, which exactly coincides with the assigned vibrational frequency of 500 cm^{-1} . Moreover, the population dynamics of the states $|\tilde{A}\rangle$ and $|\tilde{B}\rangle$ is shown in Fig. 3 (C) by summing the wave packet population along the reaction coordinate Q_- . Spectral information can be again obtained from the Fourier transform. In Fig. 3 (D), the vibrational coherence is identified by the narrow peaks at 500 cm^{-1} and 1000 cm^{-1} , which coincide with the results from the 2D spectroscopic calculations

shown in Fig. 2. In addition, a broadband background with a maximum at 200 cm^{-1} and with small magnitude is visible, which again provides evidence of the electronic coherence being short-lived.

The resonant case, with $\Omega = 200 \text{ cm}^{-1}$, is addressed in Fig. 3 (E) to (F). Compared to the off-resonant case, no significant difference occurs. The initial wave packet in the excited state $|\tilde{A}\rangle$ is transferred to $|\tilde{B}\rangle$ over time. The only difference is the vibrational oscillation period of ~ 165 fs. The integrated time-dependent populations are shown in Fig. 3 (G) and the associated spectral information in Fig. 3 (H). One narrow peak at 200 cm^{-1} and one additional peak at 400 cm^{-1} with quite small magnitude occur. Also here, the result agrees with the observation of the 2D spectroscopic calculations in Fig. 1.

Vibronic dimer under weak electronic dephasing Up to here, we have studied realistic parameters of the electronic dephasing and the vibrational damping constants. The possibility remains that for weaker electronic dephasing, the role of a coherent vibronic coupling could be more pronounced. That this is not the case follows from the dynamics of a vibronic dimer in the off-resonant case with $\Omega = 500 \text{ cm}^{-1}$ under (unrealistically) weak electronic dephasing. For this, we set $\gamma^{\text{el}} = \gamma^{\text{vib}} = 0.02$, and $\omega_c = 50 \text{ cm}^{-1}$. The wave packet dynamics projected to the PESs of $|\tilde{A}\rangle$ and $|\tilde{B}\rangle$ is shown in Fig. 4 (A) and (B), respectively. The purely vibrational coherence can be seen from the wave packet oscillations around $Q_- = -1.5$ with a period of ~ 67 fs, which coincides with the vibrational period. The electronic coherence is visible in Fig. 4 as a large-amplitude population exchange between the two electronic states. The electronic oscillation period of ~ 167 fs corresponds to the electronic energy gap $\Delta E = 200 \text{ cm}^{-1}$ in the adiabatic basis.

Thus, the large-amplitude exchange is caused by the superposition of the wave packet components on the two PESs. To reveal the oscillation components and their lifetimes, we sum the wave packet components along the reaction coordinate and plot it in Fig. 4 (C). The Fourier spectrum is shown in Fig. 4 (D). Two large peaks at 200 cm^{-1} and 500 cm^{-1} correspond to the oscillations due to electronic and vibrational coherence, respectively. Two small vibronic peaks at $500 - 200 = 300 \text{ cm}^{-1}$ and $500 + 200 = 700 \text{ cm}^{-1}$ are due to the vibronic mixing. Most importantly, although the frequencies indeed mix and additional peaks are generated, the line widths of the peaks at 200 cm^{-1} , 300 cm^{-1} , 500 cm^{-1} , and 500 cm^{-1} are 35 cm^{-1} , 40 cm^{-1} , 20 cm^{-1} , and 45 cm^{-1} , and are thus all comparable. This proves that the lifetime of the electronic coherence is not affected by vibronic coupling to a vibrational mode.

Impact of coherent vibronic coupling on anticorrelated vibrations Finally, we address the possibility that a strong coherent vibronic coupling could enhance the amplitude of the anticorrelated component of the vibrational dynamics^{32,35}. The latter is given by the magnitude of the vibrational peak in the Fourier spectrum of the wave-packet dynamics, as, e.g., shown in Figs. 3 D and H and Fig. 4D. In Fig. 5, we show the amplitude of the anticorrelated vibration for increasing vibronic coupling Δ for weak ($\gamma^{\text{el}} = 0.02$) and strong ($\gamma^{\text{el}} = 0.7$) electronic dephasing. For increasing Δ , the mixing of the anticorrelated vibration with the electronic parts becomes stronger. Indeed, for weak electronic dephasing, we find an increase of the anticorrelated vibrational amplitude which confirms the picture of Refs.^{32,35}. However, for the more realistic case of stronger electronic dephasing, the amplitude of the anticorrelated vibration depends only weakly on the vibronic coupling, since the coherent electron-vibrational mixing is dephased very rapidly and does

not influence the vibration at later times.

Conclusions

In conclusion, we have shown that, under ambient physical conditions, it is irrelevant for the lifetime of electronic quantum coherence in the excitation energy transfer whether the two exciton states couple to two anticorrelated or correlated vibrational modes. This holds irrespective of whether the electronic and the vibrational transitions are resonant or off-resonant and follows from an analysis of a model dimer in which each excited state is coupled to its own vibrational mode in an anticorrelated manner. Two independent baths for electronic dephasing as well as vibrational damping are included. By this, we answer a key question in the literature³¹ whether a coupling to a long-lived vibrational mode can lead to a substantial increase of the electronic coherence time. The conclusions are drawn from the calculated dynamics, the 2D electronic spectra and the subsequent 2D global fitting approach. The exciton dynamics is characterized by the combination of a fast electronic dephasing and a long-lived vibrational coherent component, which has very small oscillation amplitudes. The long-lived oscillations are solely due to the coherence between different vibrational levels, irrespective of a resonant or an off-resonant vibronic anticorrelated coupling. Even under (unrealistically) weak electronic dephasing, the electronic coherence lifetime is not enhanced by the vibronic components. The same conclusion has been drawn from the study of indocarbocyanine dye molecules³³. In addition, we find that a strong mixing of electronic and anticorrelated vibrational components of the wavefunction due to strong vibronic coupling does not enhance the vibrational amplitude at long times under ambient conditions. This effect only

can occur under unrealistically weak electronic dephasing^{32,35}, but does not play a role in realistic physical systems, the reason being that the required coherent vibronic mixing is rapidly destroyed by fast electronic dephasing.

1. Blankenship RE (2014) Antenna complexes and energy transfer processes. *Molecular Mechanisms of Photosynthesis* (Blackwell Science, Oxford/Malden, 2002), pp 61-94.
2. Jonas DM (2003) Two-dimensional femtosecond spectroscopy. *Annu Rev Phys Chem* 54:425-463.
3. Cowan ML, Ogilvie JP, Miller RJD (2004) Two-dimensional spectroscopy using diffractive optics based phased-locked photon echoes. *Chem Phys Lett* 386:184-189.
4. Brixner T, Mančal T, Stiopkin IV, Fleming GR (2004) Phase-stabilized two-dimensional electronic spectroscopy. *J Chem Phys* 121:4221-4236.
5. Mukamel S (1995) Nonlinear response functions and optical susceptibilities. *Principles of Nonlinear Optical Spectroscopy* (Oxford Univ Press, Oxford), pp 111-139.
6. Engel GS, et al. (2007) Evidence for wavelike energy transfer through quantum coherence in photosynthetic systems. *Nature* 446:782-786.
7. Panitchayangkoon G, et al. (2010) Long-lived quantum coherence in photosynthetic complexes at physiological temperature. *Proc Natl Acad Soc USA* 107:12766-12770.
8. Lambert N, Chen YN, Cheng YC, Li CM, Chen GY, Nori F (2013) Quantum biology. *Nat Phys* 9:10-18.

9. Collini E, Wong CY, Wilk KE, Curmi PMG, Brumer P, Scholes GD (2010) Coherently wired light-harvesting in photosynthetic marine algae at ambient temperature. *Nature* 463:644-647.
10. Schlau-Cohen GS, et al. (2012) Elucidation of the timescales and origins of quantum electronic coherence in LHCII. *Nat. Chem.* 4:389-395.
11. Fuller FD, Pan J, Gelzinis A, Butkus V, Senlik SS, Wilcox DE, Yocum CF, Valkunas L, Abramavicius D, Ogilvie JP (2014) Vibronic coherence in oxygenic photosynthesis. *Nat Chem* 6:706-711.
12. Romero E, Augulis R, Novoderezhkin VI, Ferretti M, Thieme J, Zigmantas D, van Grondelle R (2014) Quantum coherence in photosynthesis for efficient solar-energy conversion. *Nat Phys* 10:676-682.
13. Ishizaki A, Fleming GR (2009) Theoretical examination of quantum coherence in a photosynthetic system at physiological temperature. *Proc Natl Acad Soc USA* 106:17255-17260.
14. Plenio MB, Almeida J, Huelga SF (2013) Origin of long-lived oscillations in 2D-spectra of a quantum vibronic model: electronic versus vibrational coherence. *J Chem Phys* 139:235102.
15. Adolphs J, Renger T (2006) How proteins trigger excitation energy transfer in the FMO complex of green sulfur bacteria. *Biophys J* 91:2778-2797.
16. Wendling M, Pullerits T, Przyjalowski MA, Vulto SIE, Aartsma TJ, van Grondelle R, van Amerongen H (2000) Electron-Vibrational Coupling in the Fenna-Matthews-Olson Complex of *Prosthecochloris aestuarii* Determined by Temperature-Dependent Absorption and Fluorescence Line-Narrowing Measurements. *J Phys Chem B* 104:5825-5831.

- Adolphs J, Renger T (2006) How proteins trigger excitation energy transfer in the FMO complex of green sulfur bacteria. *Biophys J* 91:2778-2797.
17. Chen L, Zheng R, Jing Y, Shi Q (2011) Simulation of the two-dimensional electronic spectra of the Fenna-Matthews-Olson complex using the hierarchical equations of motion method. *J Chem Phys* 134:194508.
 18. Nalbach P, Braun D, Thorwart M (2011) Exciton transfer dynamics and quantumness of energy transfer in the Fenna-Matthews-Olson complex. *Phys Rev E* 84:041926.
 19. Wu J, Liu F, Ma J, Silbey RJ, Cao JS (2012) Efficient energy transfer in light-harvesting systems: Quantum-classical comparison, flux network, and robustness analysis. *J Chem Phys* 137:174111.
 20. Lee MK, Coker DF (2016) Modeling Electronic-Nuclear Interactions for Excitation Energy Transfer Processes in Light-Harvesting Complexes. *J Phys Chem Lett* 7:3171-3178.
 21. Lee MK, Huo P, Coker DF (2016) Semiclassical Path Integral Dynamics: Photosynthetic Energy Transfer with Realistic Environment Interactions. *Annu Rev Phys Chem* 67: 639-668.
 22. Oh SA, Coker DF, Hutchinson DAW (2018) Optimization of energy transport in the Fenna-Matthews-Olson complex via site-varying pigment-protein interactions. arXiv:1807.03459.
 23. Chandrasekaran S, Agtar M, Valleau S, Aspuru-Guzik A, Kleinekathöfer U (2015) Influence of Force Fields and Quantum Chemistry Approach on Spectral Densities of BChl a in Solution and in FMO Proteins. *J Phys Chem B* 119:9995-10004.

24. Olbrich C, Strümpfer J, Schulten K, Kleinekathöfer U (2011) Theory and Simulation of the Environmental Effects on FMO Electronic Transitions. *J Phys Chem Lett* 2:1771-1776.
25. Duan HG, et al. (2017) Nature does not rely on long-lived electronic quantum coherence for photosynthetic energy transfer. *Proc Natl Acad Soc USA* 114:8493-8498.
26. Egorova D (2014) Self-analysis of coherent oscillations in time-resolved optical signals. *J Phys Chem A* 118:10259-10267.
27. Butkus V, et al. Vibrational vs. electronic coherences in 2D spectrum of molecular systems. *Chem Phys Lett* 545:40-43.
28. Seibt J, Pullerits T (2013) Beating signals in 2D spectroscopy: electronic or nuclear coherences? application to a quantum dot model system. *J Phys Chem C* 117:18728-18737.
29. Kreisbeck C, Kramer T (2012) Long-lived electronic coherence in Dissipative exciton dynamics of light-harvesting complexes. *J Phys Chem Lett* 3:2828-2833.
30. Kreisbeck C, Kramer T, Aspuru-Guzik A (2013) Disentangling electronic and vibronic coherences in two-dimensional echo spectra. *J Phys Chem B* 117:9380-9385.
31. Chin AW, et al. (2013) The role of non-equilibrium vibrational structures in electronic coherence and recoherence in pigmentprotein complexes, *Nat Phys* 9:113-118.
32. Tiwari V, Peters WK, Jonas DM (2013) Electronic resonance with anticorrelated pigment vibrations drives photosynthetic energy transfer outside the adiabatic framework. *Proc Natl Acad Soc USA* 110:1203-1208.

33. Duan HG, et al. (2015) On the origin of oscillations in two-dimensional spectra of excitonically-coupled molecular systems. *New J Phys* 17:072002.
34. Halpin A, et al. (2014) Two-dimensional spectroscopy of a molecular dimer unveils the effects of vibronic coupling on exciton coherences. *Nat Chem* 6:196-201.
35. Yeh S-H, Hoehn RD, Allodi MA, Engel GS, Kais S (2018) Elucidation of near-resonance vibronic coherence lifetimes by nonadiabatic electronic-vibrational state character mixing. *Proc Natl Acad Soc USA*, Article Ahead of Print, <https://doi.org/10.1073/pnas.1701390115>
36. Gelin MF, et al. (2012) Bath-induced correlations and relaxation of vibronic dimers. *J Chem Phys* 136:034507.
37. Manthe U, Köppel H (2009) Dynamics on potential energy surfaces with a conical intersection: Adiabatic, intermediate, and diabatic behavior. *J Chem Phys* 93:1658-1669.
38. Qi D, Duan HG, Sun ZL, Miller RJD, Thorwart M (2017) Tracking an electronic wave packet in the vicinity of a conical intersection. *J Chem Phys* 147:074101.
39. Meier C, Tannor DJ (1999) Non-Markovian evolution of the density operator in the presence of strong laser fields. *J Chem Phys* 111:3365-3376.
40. Kleinekathöfer U (2004) Non-Markovian theories based on a decomposition of the spectral density. *J Chem Phys* 121:2505-2514.
41. Cheng YC, Fleming GR (2008) Coherence quantum beats in two-dimensional electronic spectroscopy. *J Phys Chem A* 112:4254-4260.

42. Gelin MF, Egorova D, Domcke W (2005) Efficient method for the calculation of time- and frequency-resolved four-wave mixing signals and its application to photon-echo spectroscopy. *J Chem Phys* 123:164112.

Acknowledgements We acknowledge financial support by the Max Planck Society and the Hamburg Centre for Ultrafast Imaging (CUI) within the German Excellence Initiative supported by the Deutsche Forschungsgemeinschaft. H-G.D. acknowledges generous financial support by the Joachim-Hertz-Stiftung Hamburg.

Significance Statement We have studied the impact of molecular vibrations on the electronic coherence during the energy transfer in a model dimer. The full dynamics are revealed in the calculated 2D electronic spectra. We show that the long-lived coherence present in the off-diagonal spectral signals is solely due to vibrational coherence in the monomer. Our calculations illustrate that neither the electronic coherence between two monomers can be enhanced by vibrations of individual pigments, irrespective of resonant or off-resonant conditions, nor can a coherent vibronic coupling enhance the amplitude of the anticorrelated vibrational mode under realistic conditions.

Supporting Information The Supplementary Information includes the global fitting approach and results, low-temperature calculations and vibrational dynamics of monomer.

Competing Interests The authors declare that they have no competing financial interests.

Correspondence michael.thorwart@physik.uni-hamburg.de and dwayne.miller@mpsd.mpg.de

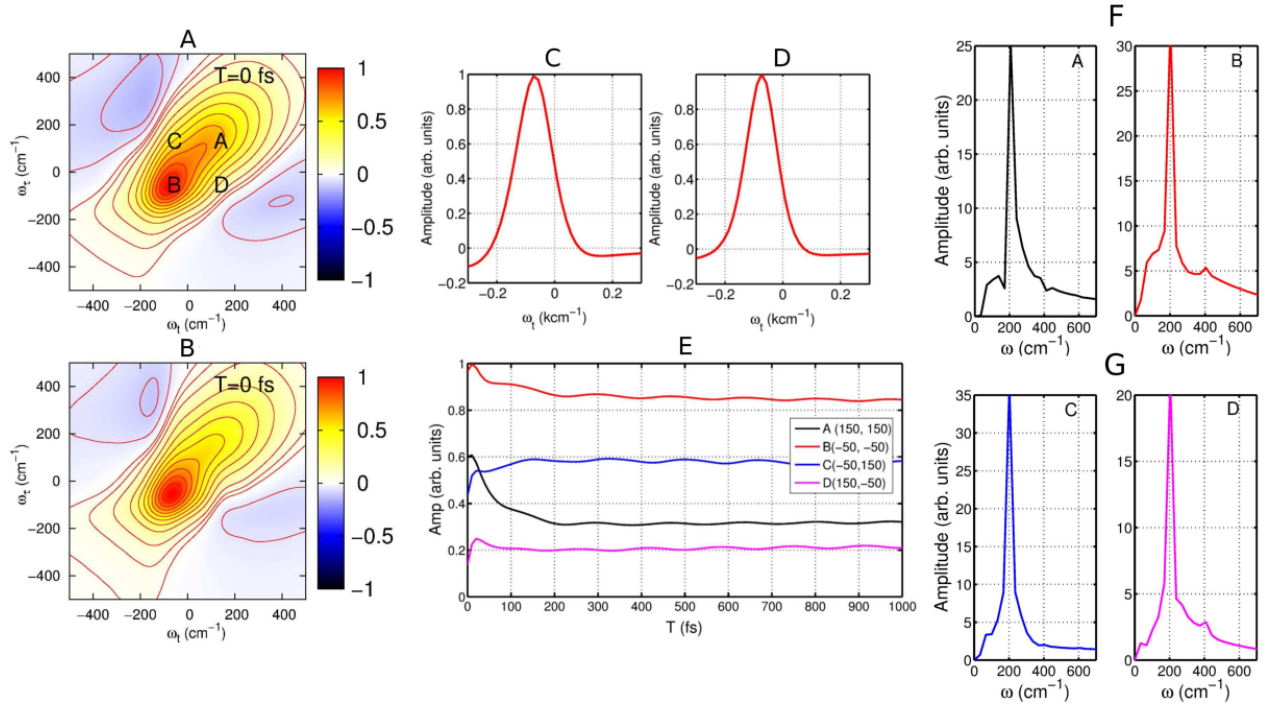


Figure 1: (A) Real part of the 2D electronic spectrum of the vibronic dimer at room temperature (300 K). The diagonal peak A is located at $(\omega_t = 150 \text{ cm}^{-1}, \omega_\tau = 150 \text{ cm}^{-1})$ and B at $(\omega_t = -50 \text{ cm}^{-1}, \omega_\tau = -50 \text{ cm}^{-1})$. The off-diagonal peak C sits at $(\omega_t = -50 \text{ cm}^{-1}, \omega_\tau = 150 \text{ cm}^{-1})$ and D at $(\omega_t = 150 \text{ cm}^{-1}, \omega_\tau = -50 \text{ cm}^{-1})$. The time dependent trace of the selected peaks are shown in (E). For comparison, the 2D spectrum of the dimer without the effective vibrational mode is shown in (B). To obtain the timescale of the electronic dephasing, the anti-diagonal profile of the peaks B in (A) and (B) are shown in (C) and (D). The resulting timescale of the electronic dephasing is 70 fs and 80 fs, respectively. (F), (G) Power spectra of the peaks A, B, C, and D for the case with vibrational coupling. The broad background spectral band is associated to fast electronic dephasing. In addition to the strong vibrational peak at 200 cm^{-1} , one additional peak at 400 cm^{-1} is well resolved.

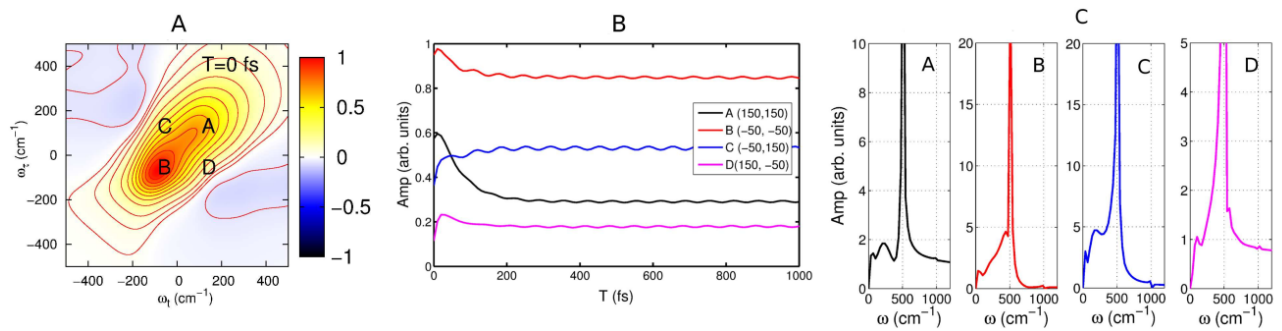


Figure 2: (A) Real part of the 2D electronic spectrum of the vibronic dimer under off-resonant conditions with $\Omega = 500 \text{ cm}^{-1}$ at $T = 0 \text{ fs}$. The kinetics of the selected peaks at A, B, C, and D are shown in (B), the associated power spectra are shown in (C). To resolve the lifetime of the electronic coherence, we fit the broad peak at 200 cm^{-1} with the Lorentzian lineshape and obtain the electronic coherence time of $\sim 70 \text{ fs}$, which agrees with the resonant case.

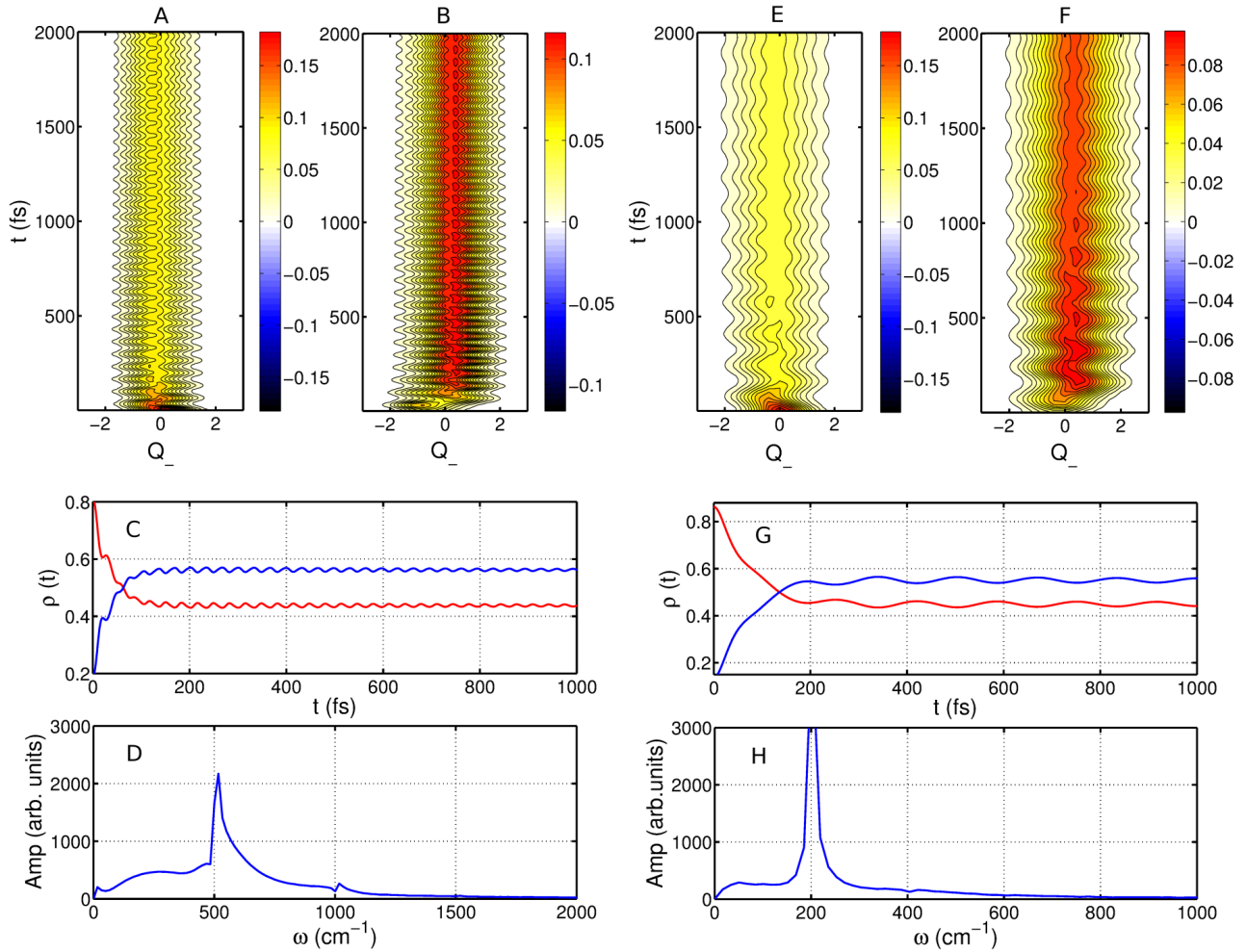


Figure 3: Time evolution of the wave-packet in the excited states $|\tilde{A}\rangle$ (A) and $|\tilde{B}\rangle$ (B). The integrated populations of the electronic states $|\tilde{A}\rangle$ and $|\tilde{B}\rangle$ obtained by summing along the reaction coordinate Q_- are shown in (C), together with the Fourier transform of the residuals in (D). The long-lived vibrational coherence is identified by the narrow peaks at 500 cm^{-1} and 1000 cm^{-1} . In addition, one broadband peak at 200 cm^{-1} represents short-lived electronic coherence. The corresponding results of the resonant case are shown in (E) to (H), respectively. The long-lived vibrational coherence can be identified by the narrow peak and 200 cm^{-1} and the small peak at 400 cm^{-1} .

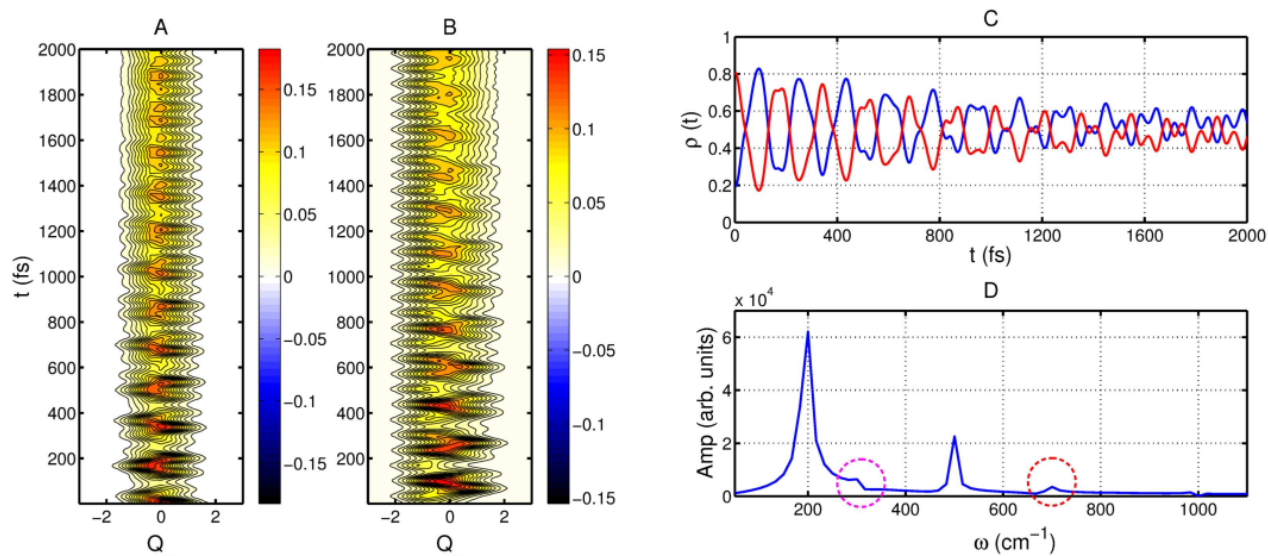


Figure 4: Time evolution of the wave-packet on the excited state PESs for $|\tilde{A}\rangle$ is shown in (A) and for $|\tilde{B}\rangle$ in panel (B) for the vibronic dimer under off-resonant conditions for very weak electronic dephasing $\gamma^{\text{el}} = \gamma^{\text{vib}} = 0.02$, and $\omega_c = 50 \text{ cm}^{-1}$. The integrated populations of the electronic states $|\tilde{A}\rangle$ and $|\tilde{B}\rangle$ obtained by summing along the reaction coordinate Q_- are shown in (C), together with the Fourier transform of the residuals shown in (D). The vibronic coherence can be identified by the two peaks 300 cm^{-1} and 700 cm^{-1} , which are marked by circles.

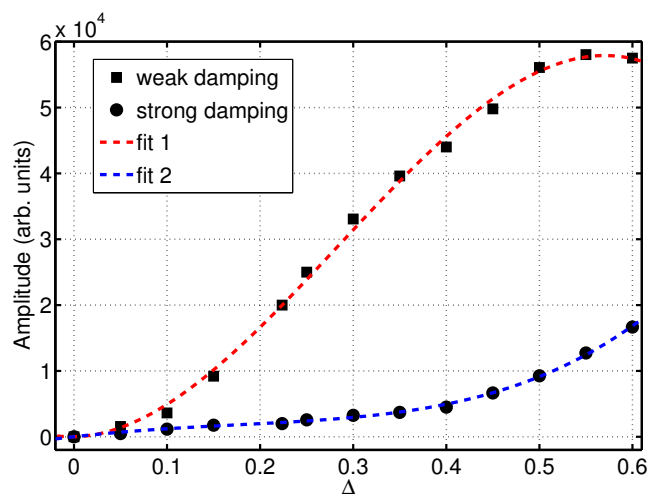


Figure 5: Oscillation amplitude of the anticorrelated vibration vs. the vibronic coupling strength Δ for weak ($\gamma^{\text{el}} = 0.02, \omega_c = 50 \text{ cm}^{-1}$) and strong ($\gamma^{\text{el}} = 0.7, \omega_c = 350 \text{ cm}^{-1}$) electronic dephasing for $\Delta E = 200 \text{ cm}^{-1}$, $\Omega = 500 \text{ cm}^{-1}$, and $T = 300 \text{ K}$.